

# Designing Spin-driven Multiferroics in Altermagnets

Ranquan Cao,<sup>1</sup> Ruizhi Dong,<sup>1</sup> Ruixiang Fei,<sup>1,\*</sup> and Yugui Yao<sup>1,†</sup>

<sup>1</sup>*Key Lab of Advanced Optoelectronic Quantum Architecture and Measurement (MOE),  
School of Physics, Beijing Institute of Technology, Beijing 100081, China*

Spin-driven multiferroics exhibit strong magnetoelectric coupling, with notable polarization changes under a magnetic field, but these effects are usually limited to high- $Z$  magnetic insulators with low electronic polarization. In this work, we introduce altermagnets as a promising platform for achieving strong magnetoelectric coupling in low- $Z$  systems with substantial polarization. This large polarization arises from a design principle that utilizes the Heisenberg-like exchange striction mechanism, eliminating the reliance on spin-orbit coupling (SOC). This approach enables the Kramers-degenerate antiferromagnetic phase derived from altermagnetic insulators to achieve substantial polarization without spin splitting, providing a flexible platform for regulating spin-splitting phenomena. Through first-principles simulations and an effective Landau-Ginzburg Hamiltonian, we demonstrate that materials in the LiMnO<sub>2</sub> family and strained RuF<sub>4</sub> family can achieve polarization values exceeding  $1.0 \mu\text{C}/\text{cm}^2$ , an order of magnitude larger than those found in SOC-driven multiferroics. Moreover, their magnetoelectric coupling is one to two orders of magnitude stronger than that observed in conventional multiferroics and those driven by SOC.

**Introduction**—Multiferroics, primarily involving the coexistence of magnetism and ferroelectricity, have garnered significant attention due to their intriguing physics and the potential to drive faster, smaller, energy-efficient data storage [1–3]. In particular, type II multiferroics, characterized by a strong coupling between magnetic properties and magnetically induced ferroelectricity, are crucial for controlling electronic polarization using magnetic fields and vice versa. [4, 5]. To date, three primary approaches for generating type II multiferroic have been identified, categorized into spin-orbit coupling (SOC)-related and SOC-unrelated cases [2, 6–8]. The SOC-related phenomena involve mechanisms such as the Dzyaloshinskii–Moriya (DM) interaction [9, 10] and spin-dependent metal–ligand  $p$ - $d$  hybridization [11–13]. In these cases, the polarization values are strongly correlated with the strength of the SOC, which typically requires the presence of heavy elements. However, this relativistic effect is often weak, leading to relatively modest electronic polarization. For instance, the DM and inverse DM mechanisms induced ferroelectricity in orthorhombic TbMnO<sub>3</sub> [4] and CaMn<sub>7</sub>O<sub>12</sub> [14], generally yielding polarization values below  $0.1 \mu\text{C}/\text{cm}^2$ , with a maximum reported polarization of  $0.3 \mu\text{C}/\text{cm}^2$  [14, 15].

The SOC-unrelated case refers to the Heisenberg-like exchange striction mechanism, which requires a commensurate spin order and low symmetry in the specific chemical lattice, but does not involve SOC [16]. In contrast to the SOC-dependent mechanism, exchange striction in collinear magnets can be much more pronounced, leading to a substantial increase in polarization. For example, a polarization of around  $0.1 \mu\text{C}/\text{cm}^2$  has been reported in compressed orthorhombic TbMnO<sub>3</sub> [17] when the DM mechanism transitions to an exchange striction mechanism. Unfortunately, only a limited number of oxide materials, such as TbMn<sub>2</sub>O<sub>5</sub> [5] and orthorhombic HoMnO<sub>3</sub> [18–20], have been identified to exhibit exchange striction-induced multiferroicity.

Recent studies on altermagnetic antiferromagnet (AFM) [21–23] have unveiled fascinating phenomena, including large spin-splitting [21, 23–26] and the  $T$ -odd spin Hall effect [27]. These phenomena are independent of SOC and are instead directly driven by the collinear spin alignment that satisfies the commensurate spin order required by the exchange striction mechanism [6]. Moreover, planar or bulk  $d$ -wave and  $g$ -wave altermagnetic materials, which typically exhibit low symmetry (e.g., two-fold or three-fold) [24], provide excellent platforms for exploring potential spin-induced multiferroicity via the exchange striction mechanism. Additionally, the spin conservation and pronounced spin splitting in altermagnets make it ideal for spintronic applications. The combination of altermagnetic and multiferroic properties is highly beneficial, as it allows for efficient control of spin-related phenomena using electric or magnetic fields.

In this study, we propose that a spin-induced multiferroic can be generated from the altermagnetic phase. Our results show that, within the supercell structure, the collinear multiferroic phase is a Kramers-degenerate AFM phase, exhibiting spin-down and spin-up degeneracy and a significant spontaneous electronic polarization driven by exchange striction. Due to the spin-induced ferroelectricity, electric or magnetic fields can rapidly switch between different magnetic phases, such as ferromagnetic, altermagnetic, and Kramers-degenerate AFM, providing potential for various applications. Using first-principles simulations and an effective Landau-Ginzburg Hamiltonian, we reveal that LiMnO<sub>2</sub> and strained RuF<sub>4</sub> materials can achieve polarization above  $1.0 \mu\text{C}/\text{cm}^2$  with magnetoelectric coupling far exceeding conventional and SOC-driven multiferroics.

**Spin-induced ferroelectricity and phase diagram:** Motivated by the exploration of exchange striction-induced

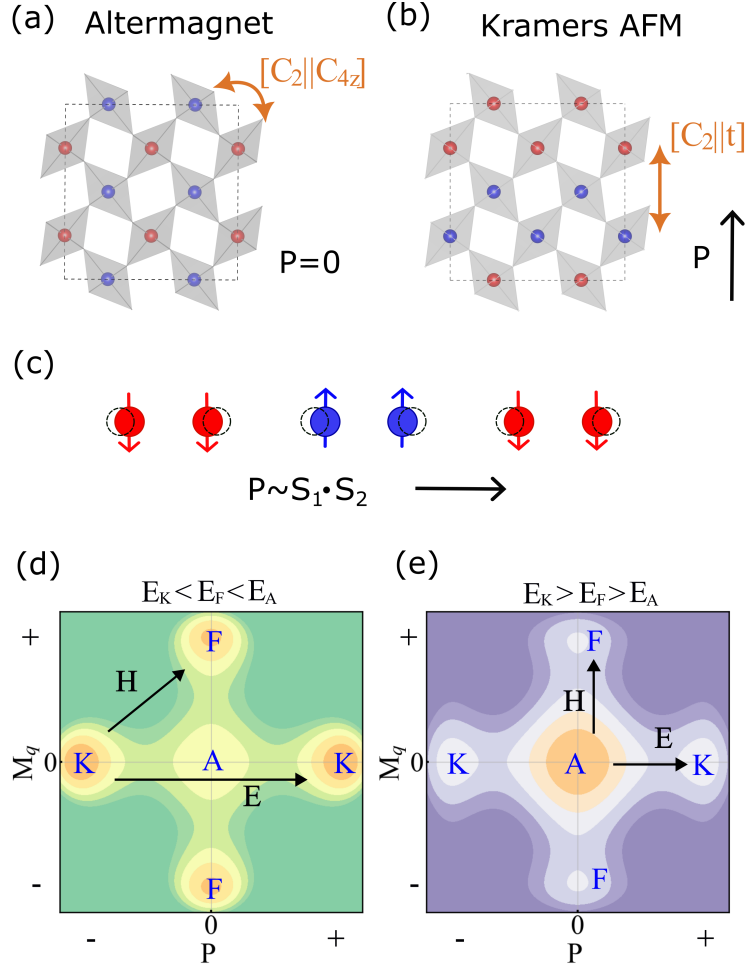


FIG. 1. Atomic structure showing only the magnetic atoms, with the spin pattern in (a) representing the altermagnetic phase and in (b) representing the Kramers-degenerate AFM phase. (c) Spin pattern along the  $y$ -direction in (b) showing a Peierls-like phase transition. Phase diagrams for the Kramers-degenerate AFM (d) and altermagnetic (e) as ground states, with K, A, and F representing Kramers-degenerate AFM, altermagnetic, and ferromagnetic phases, respectively.

multiferroic properties in  $\text{HoMnO}_3$  [18, 19], we designed a spin structure within a  $2 \times 2$  supercell of an altermagnet. In Fig. 1(a), the red and blue atoms represent spin-up and spin-down magnetic moments, respectively, connected by the  $[C_2||C_{4z}]$  spin transformation. Here, the  $C_2$  denotes a  $180^\circ$  rotation in the spin-only space, while the  $C_{4z}$  transformation involves proper or improper fourfold rotations in real space [24]. This spin transformation causes the spin-up and spin-down bands to split, yet the electron polarization remains zero due to space inversion symmetry. We design the spin structure in a zigzag arrangement, with spins represented by the blue and red atoms in Fig. 1(b). Notably, the spin-up and spin-down sublattices are connected by the spin transformation  $[C_2||t]$ , where  $t$  represents a half-unit translation symmetry in real space. This symmetry maintains the degeneracy of spin-up and spin-down bands across the entire reciprocal space, classifying the structure as a Kramers-degenerate AFM (type II AFM).

We observe that the electronic polarization of this spin structure is oriented along the  $y$ -axis, as shown in Fig. 1(b). This polarization arises from two contributions: one due to the inversion symmetry breaking induced by the spin pattern, and the other from the ionic component. As depicted in Fig. 1(c), the spin pattern disrupts space inversion symmetry. Concurrently, the crystal-field-modified super-exchange interaction facilitates an attractive interaction between parallel spins and a repulsive interaction between antiparallel spins. This mechanism drives the ions to undergo a Peierls-like structural phase transition, leading to a moderate polarization along the  $y$ -axis. If the free energy of this Kramers-degenerate AFM configuration is significantly lower than that of the altermagnetic phase, the material could exhibit stable multiferroic behavior with strong magnetoelectric coupling.

Regardless of which phase is the ground state, the Hamiltonian can be expressed in the Landau-Ginzburg form:

$$H = \frac{1}{2}a_p(\eta)P^2 + \frac{1}{4}b_p(\eta)P^4 + \frac{1}{6}c_p(\eta)P^6 + \frac{1}{2}a_q(\eta)M_q^2 + \frac{1}{4}b_q(\eta)M_q^4 + \frac{1}{6}c_q(\eta)M_q^6 + \frac{1}{2}\lambda(\eta)M_q^2P^2 - EP \quad (1)$$

Here, we focus on the spin-induced polarization  $P$ . For each strain  $\eta$  and external electric field  $E$ , the ground state is determined by minimizing the free energy with respect to  $P$  and  $M_q$ . The magnetic order parameter  $M_q$  is defined as:  $M_q = \frac{1}{N} \sum_j e^{iq \cdot R_j} \langle S_j \rangle$ , where  $\langle S_j \rangle$  is the thermodynamic average of the normalized spin at the site  $R_j$  and  $N$  is the number of spins. Taking  $\text{MnF}_2$  as an example,  $q = \pi(0, 0, \frac{2}{c})$  stands for the altermagnetic phase, and  $q = \pi(\frac{2}{a}, \frac{1}{a}, \frac{1}{c})$  corresponds to the Kramers-degenerate AFM. The parameter  $\lambda(\eta)$  denotes the magnetoelectric coupling strength under the specified strain  $\eta$ . Using this Hamiltonian, a phase diagram can be constructed to depict the transitions between the Kramers-degenerate AFM phase, the altermagnetic phase, and the ferromagnetic phase.

Two primary scenarios can be identified: one where the Kramers-degenerate AFM phase is the ground state, and another where the altermagnetic phase serves as the ground state. In Fig. 1(d), the spontaneously polarized Kramers-degenerate AFM serves as the ground state, allowing the electric field to switch the negatively polarized state to a positively polarized structure. Concurrently, an applied magnetic field can drive a transition from the Kramers-degenerate AFM to a non-polarized ferromagnetic phase, leading to strong magnetoelectric coupling. In the second scenario, shown in Fig. 1(e), the altermagnetic phase is the ground state. Upon the application of an electric field, the system transitions from the altermagnetic phase to a Kramers-degenerate AFM phase. While the net magnetization remains unchanged, the suppression of spin splitting results in the vanishing of phenomena typically associated with altermagnets, such as the  $T$ -even symmetric spin Hall effect. Similarly, applying a magnetic field can diminish spin splitting within the altermagnetic phase, causing the spin Hall effect to transform into the anomalous Hall effect.

**Materials realizations:** Non-collinear spin alignment in antiferromagnets can spontaneously break inversion symmetry, leading to spin-driven ferroelectricity [28]. However, the DM interaction, arising from SOC, can also promote non-collinear spin configurations, making it challenging to disentangle the contributions of non-SOC mechanisms to spin-driven ferroelectricity [9, 10]. Moreover, these systems generally display weak electronic polarization, restricting their utility in multiferroic applications. To address this, we focus on collinear systems to investigate spin-driven ferroelectricity, magnetoelectric coupling, and potential phase transitions. Our first-principles calculations [29] reveal that numerous materials identified as  $g$ -wave or  $d$ -wave altermagnets, which possess lower crystal symmetry compared to  $i$ -wave altermagnets, can transition into Kramers-degenerate antiferromagnets, functioning as spin-induced multiferroics.

A representative example is the  $\text{LiMnO}_2$  family, which includes  $\text{NaMnO}_2$  compounds. These structures can be described as Li (or Na) ions intercalated into  $\text{MnO}_2$  frameworks, a hallmark of ionic battery materials [30]. First-principles calculations reveal that several experimentally observed phases of  $\text{LiMnO}_2$  family display altermagnetic behavior, with the orthorhombic  $\text{LiMnO}_2$  (Pmnm) and  $\text{NaMnO}_2$  ( $I4_1/amd$ ) phases being notable examples. However, achieving a transition from the altermagnetic phase to a Kramers-degenerate phase in these materials necessitates lattice compression or strain exceeding 8%, posing substantial experimental challenges.

The DFT+U calculations [29, 31–34] identify the Kramers-degenerate phase in the stable  $P2_12_12$  configuration as the ground state. Fig. 2(a) presents the corresponding Brillouin zone and the band structure of the Kramers-degenerate AFM. The spin-up and spin-down band degeneracy originates from the half-unit translation operator connecting the spin-down and spin-up sublattices, consistent with the mechanism illustrated in Fig. 1(b). In contrast, in the altermagnetic phase, the operator  $[C_2|C_{2z}]$  connects the spin-down and spin-up sublattices, resulting in spin splitting outside the high-symmetry plane, as indicated by the green shading in the inset of Fig. 2(b). This behavior classifies the system as a planar  $g$ -wave altermagnet.

We derived the phase diagram from the effective Hamiltonian in Eq. (1) by calculating various spin configurations using the DFT+U method [29]. The K, A, and F phases represent the Kramers-degenerate AFM, altermagnetic, and ferromagnetic phases, respectively, with green and purple octahedra in the lower panel of Fig. 2(c) denoting spin-up and spin-down sites. Our calculations reveal that the ground state of this structure is a Kramers-degenerate AFM with a polarization of  $P = 0.1 \mu\text{C}/\text{cm}^2$ , arising from both the spin pattern and a spin-induced Peierls-like structural transition. When calculating the polarization for the Kramers-degenerate spin configuration with fixed atomic positions, excluding the Peierls-like transition, we find a value of  $0.8 \mu\text{C}/\text{cm}^2$ , nearly an order of magnitude larger than that from SOC-related mechanisms.

The electromagnetic coupling constant,  $\lambda$ , is derived from Eq. (1) and quantifies the overall ability to control electronic polarization with a magnetic field, or vice versa. Fig. 2(d) illustrates how the electromagnetic coupling constant varies with biaxial strain or compression. Intuitively, the strain would affect this constant, as it alters atomic

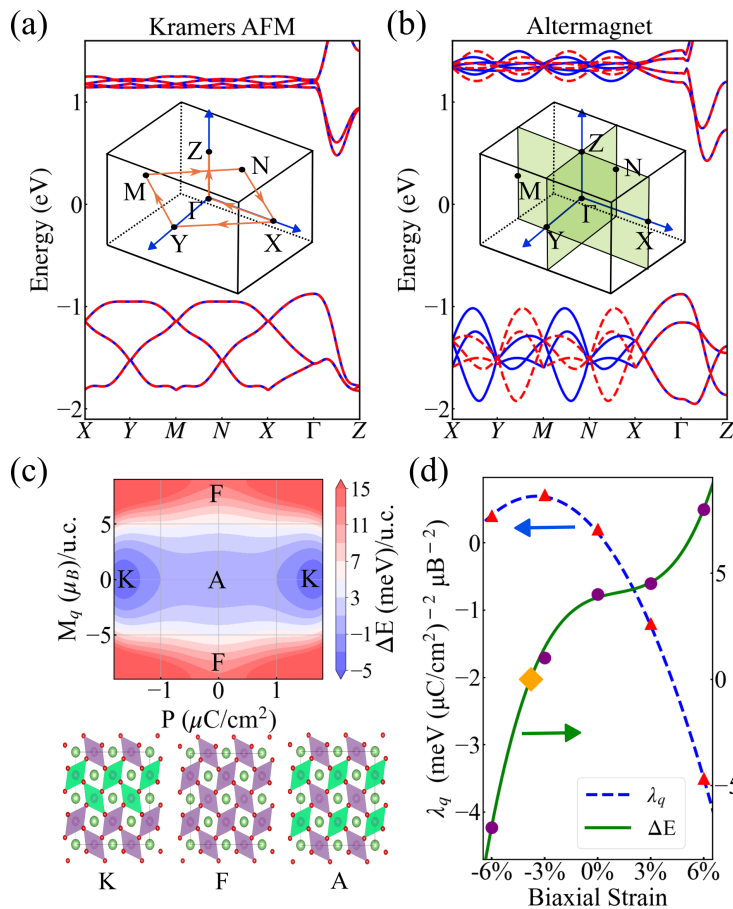


FIG. 2. (a) Band structure of the Kramers-degenerate AFM phase and (b) the altermagnetic phase. The green-highlighted plane in (b) indicates the spin-degenerate plane of the altermagnet. (c) Phase diagram of  $\text{LiMnO}_2$ , showing the Kramers-degenerate AFM (K), altermagnetic (A), and ferromagnetic (F) phases. (d) Magnetoelectric coupling constant (blue dashed line) and the energy difference between the A and K phases (green solid line), with the transition point indicated by the diamond symbol.

distances and the Mn-O-Mn angle, both of which can significantly influence the Heisenberg exchange interaction. The intrinsic magnetoelectric coupling near the Kramers-degenerate antiferromagnetic phase is approximately  $0.1 \text{ meV} \cdot \left(\frac{\mu\text{C}}{\text{cm}^2}\right)^{-2} \mu_B^{-2}$ , which is one to two orders of magnitude greater than that driven by conventional or SOC mechanisms [35–37]. We find that the magnitude of the magnetoelectric coupling can increase by an order of magnitude under moderate strain, such as a 3% lattice strain. Notably, a compressive strain of 4% or greater can shift the ground state from a Kramers-degenerate multiferroic to an altermagnetic phase, as marked by the yellow diamond symbol on the green line in Fig. 2(d).

Another notable example is the  $\text{XF}_4$  family ( $X=\text{Ru, V, Os}$ ), crystallizing in the  $P2_1/c$  space group and has been recognized as experimentally stable van der Waals-bonded bulk crystals [38, 39]. This structure has the spin group  $2_2'/2m$ , where spin-up and spin-down sublattices are related by the transformations  $[C_2||C_{2z}]$  and  $[C_2||M_z]$ . With the  $C_{2z}$  axis and  $M_z$  plane being orthogonal and no mirror plane parallel to the  $C_{2z}$  axis, the only spin-splitting off-nodal plane is the  $\Gamma MK$  plane, as shown in Fig. 3(a). This feature distinguishes it from typical  $d$ -wave altermagnets. Specifically, the band structure along the  $\Gamma Z$  line remains spin-degenerate (Fig. 3(b)) due to the symmetry enforced by the  $C_{2z}$  rotation axis.

Similar to the  $\text{LiMnO}_2$  family, the Kramers-degenerate AFM phase in these materials is noncentrosymmetric, exhibiting a spontaneous polarization of up to  $1.8 \mu\text{C}/\text{cm}^2$ , as represented by the hexagonal point in Fig. 3(c). This polarization surpasses that of benchmark spin-induced multiferroics such as  $\text{TbMnO}_3$  and  $\text{TbMn}_2\text{O}_5$  by one to two orders of magnitude [4, 5]. We examine the energy transition between the Kramers-degenerate and altermagnetic phases by rotating the spin alignment, leading to distinct electronic polarization states. The ground state is found to correspond to the altermagnetic phase, which is  $10 \text{ meV}$  lower in energy per primitive cell than the Kramers-degenerate

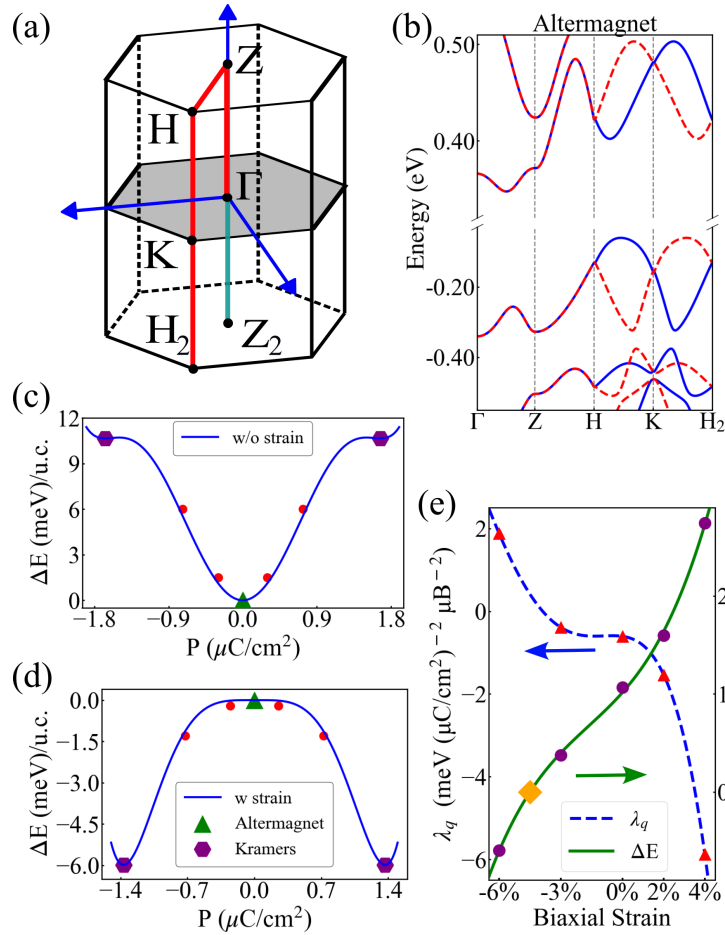


FIG. 3. (a) Brillouin zone of the  $\text{XF}_4$  family, with the spin-degenerate plane highlighted. (b) Band structure of the altermagnetic phase. (c) Energy potential for the  $M = 0$  state in the effective Hamiltonian for the intrinsic case. (d) Energy potential under 6% biaxial compression. (e) Magnetoelectric coupling constant (blue dashed line) and energy difference between the altermagnetic and Kramers-degenerate phases (green solid line) as a function of strain.

phase.

With in-plane lattice compression of the layered structure, the Kramers-degenerate AFM phase can become the ground state. As shown in Fig. 3(d), the double-well potential under 6% biaxial compression indicates the Kramers-degenerate phase as the ground state, featuring large spontaneous polarization. Biaxial compression over 4% induces a phase transition from the altermagnetic to the Kramers-degenerate phase, as shown by the green line in Fig. 3(e). By deriving the effective Hamiltonian in Eq. (1), we calculate the magnetoelectric coupling constant under various strain conditions. Under moderate strain or compression, the magnetoelectric coupling constant of the Kramers-degenerate AFM phase can reach around  $2 \text{ meV} \cdot \left(\frac{\mu\text{C}}{\text{cm}^2}\right)^{-2} \mu\text{B}^{-2}$ , an order of magnitude higher than its intrinsic value. Additionally, the two-dimensional (2D) form of the  $\text{XF}_4$  family displays similar properties, including a high magnetoelectric coupling constant [29].

Finally, we show that in specific cases, the Kramers-degenerate phase is substantially higher in energy than the ground-state altermagnetic phase, thereby hindering strain- or compression-driven transitions between the two phases. This behavior is evident in several antiferromagnetic materials, such as  $\text{MnO}_2$  and members of the  $\text{MnF}_2$  fluoride family. Notably,  $\text{MnF}_2$  has been experimentally verified to crystallize in the rutile structure with the  $P4_2/mnm$  space group [40, 41].

First-principles calculations reveal that the altermagnetic phase is about  $30 \text{ meV}$  lower in energy per primitive cell than the Kramers-degenerate phase. This altermagnetic phase belongs to the spin group  $^2_4/m^2m^1m$ , characteristic of a planar  $d$ -wave type. As illustrated in Fig. 4(a), the combined rotation operation  $[C_2|C_{4z}]$  and mirror operation  $[C_2|M_z]$  guarantee the existence of two spin-degenerate planes within the Brillouin zone.

Fig. 4(b) shows the energy potential between the Kramers-degenerate and altermagnetic phases. In the intrinsic

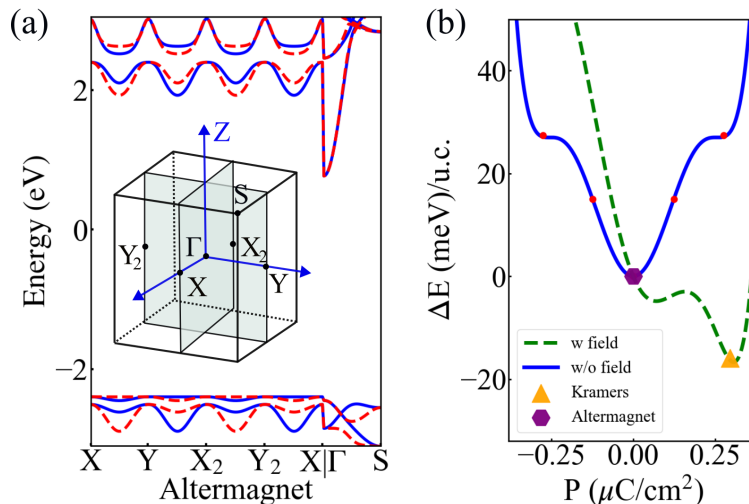


FIG. 4. (a) Band structure of the altermagnetic phase of  $\text{MnF}_2$ , with the Brillouin zone highlighting the spin-degenerate plane. (b) Energy potential of the zero total magnetic moment state for the intrinsic case (solid line) and under an applied in-plane electric field (dashed line).

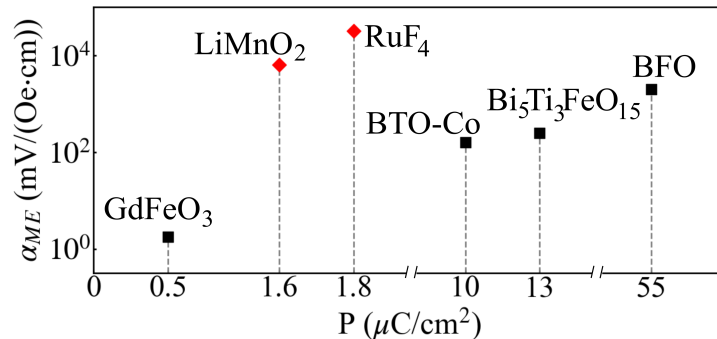


FIG. 5. Comparison of the magnetolectric coupling constants for our calculated  $\text{LiMnO}_2$  ( $P_{21}21_2$ ) and strained  $\text{RuF}_4$ , alongside representative multiferroics: BFO [36], BTO-Co [42],  $\text{Bi}_5\text{Ti}_3\text{FeO}_{15}$  [43], and  $\text{GdFeO}_3$  [37, 44].

case, the ground state corresponds to the altermagnetic phase. First-principles calculations reveal that the polarization of the Kramers-degenerate phase is  $0.25 \mu\text{C}/\text{cm}^2$ . Furthermore, we find that it is not possible to stabilize the Kramers-degenerate phase as the ground state under moderate strain or compression, such as a 15% lattice expansion or compression [29]. Instead, the phase transition between the Kramers-degenerate and altermagnetic phases can be regulated by an external electric field, as outlined in Eq. (1), due to the distinct electronic polarization of these phases.

**Giant magnetolectric coupling:** In the proposed mechanism, ferroelectricity originates from the spin alignment induced by exchange striction. This spin-dependent ferroelectric polarization exhibits strong sensitivity to external magnetic fields, enabling significant modulation and yielding a large magnetolectric coupling constant. Our calculations indicate that both  $\text{LiMnO}_2$  and strained  $\text{RuF}_4$  family exhibit significant magnetolectric coupling. As shown in Fig. 5, converting the units to  $\text{mV}/(\text{Oe} \cdot \text{cm})$  for experimental comparison [1] reveals that these materials exhibit a magnetolectric coupling constant at least an order of magnitude higher than those found in conventional and SOC-induced multiferroics.

For comparison, the ferroelectricity induced by the DM interaction in  $\text{TbMnO}_3$  serves as a prototypical example of a spin-orbit coupling (SOC)-related mechanism [4]. Although experimental values are unavailable, its magnetolectric coupling is known to be weaker than that of  $\text{BiFeO}_3$  (BFO). Similarly,  $\text{GeFeO}_3$ , another material exhibiting SOC-driven ferroelectricity [37, 44], exhibits a magnetolectric coupling constant two to three orders of magnitude lower than those of the materials we propose. While the polarization in BFO primarily arises from atomic displacement, its large magnetolectric coupling is generally attributed to the DM interaction [45]. In contrast, our proposed system, based on the exchange striction mechanism, exhibits a magnetolectric coupling constant an order of magnitude higher

than that of BFO.

In summary, we propose that the recently explored altermagnetic systems offer an ideal platform for designing spin-driven multiferroics through the exchange striction mechanism. This principle is universal for altermagnetic systems, as they inherently meet the criteria for the exchange striction mechanism: a commensurate spin order and low symmetry within the specific chemical lattice. We find that the collinear multiferroic phase is a Kramers-degenerate AFM, characterized by spin-up and spin-down degeneracy, along with a significant spontaneous polarization driven by exchange striction. Through first-principles simulations and an effective Landau-Ginzburg Hamiltonian, we show that materials such as the LiMnO<sub>2</sub> and strained RuF<sub>4</sub> families, classified as low-*Z* multiferroics, can achieve polarization values exceeding 1.0  $\mu\text{C}/\text{cm}^2$ . These materials display magnetoelectric coupling constants one to two orders of magnitude stronger than those in conventional multiferroics and SOC-driven systems. Moreover, moderate strain can effectively switch between the altermagnetic and Kramers-degenerate multiferroic phases, offering further opportunities to tune the magnetoelectric coupling.

This work is supported by the National Natural Science Foundation of China Grant No. 12204035.

---

\* rfei@bit.edu.cn

† ygyao@bit.edu.cn

- [1] W. Eerenstein, N. D. Mathur, and J. F. Scott, Multiferroic and magnetoelectric materials, *Nature* **442**, 759 (2006).
- [2] M. Fiebig, T. Lottermoser, D. Meier, and M. Trassin, The evolution of multiferroics, *Nature Reviews Materials* **1**, 16046 (2016).
- [3] R. Ramesh and N. A. Spaldin, Multiferroics: progress and prospects in thin films, *Nature Materials* **6**, 21 (2007).
- [4] T. Kimura, T. Goto, H. Shintani, K. Ishizaka, T. Arima, and Y. Tokura, Magnetic control of ferroelectric polarization, *Nature* **426**, 55 (2003).
- [5] N. Hur, S. Park, P. A. Sharma, J. S. Ahn, S. Guha, and S.-W. Cheong, Electric polarization reversal and memory in a multiferroic material induced by magnetic fields, *Nature* **429**, 392 (2004).
- [6] Y. Tokura, S. Seki, and N. Nagaosa, Multiferroics of spin origin, *Reports on Progress in Physics* **77**, 076501 (2014).
- [7] S.-W. Cheong and M. Mostovoy, Multiferroics: a magnetic twist for ferroelectricity, *Nature Materials* **6**, 13 (2007).
- [8] S. Dong, H. Xiang, and E. Dagotto, Magnetoelectricity in multiferroics: a theoretical perspective, *National Science Review* **6**, 629 (2019).
- [9] H. Katsura, N. Nagaosa, and A. V. Balatsky, Spin current and magnetoelectric effect in noncollinear magnets, *Physical Review Letters* **95**, 057205 (2005).
- [10] M. Mostovoy, Ferroelectricity in spiral magnets, *Physical Review Letters* **96**, 067601 (2006).
- [11] T. H. Arima, Ferroelectricity induced by proper-screw type magnetic order, *Journal of the Physical Society of Japan* **76**, 10.1143/JPSJ.76.073702 (2007).
- [12] H. Murakawa, Y. Onose, S. Miyahara, N. Furukawa, and Y. Tokura, Ferroelectricity induced by spin-dependent metal-ligand hybridization in ba2coge2o7, *Physical Review Letters* **105**, 137202 (2010).
- [13] H. J. Xiang, E. J. Kan, Y. Zhang, M.-H. Whangbo, and X. G. Gong, General theory for the ferroelectric polarization induced by spin-spiral order, *Physical Review Letters* **107**, 157202 (2011).
- [14] R. D. Johnson, L. C. Chapon, D. D. Khalyavin, P. Manuel, P. G. Radaelli, and C. Martin, Giant improper ferroelectricity in the ferroaxial magnet camn7o12, *Physical Review Letters* **108**, 067201 (2012).
- [15] N. Terada, Y. S. Glazkova, and A. A. Belik, Differentiation between ferroelectricity and thermally stimulated current in pyrocurrent measurements of multiferroic mmm7 o12 (m= ca, sr, cd, pb), *Physical Review B* **93**, 155127 (2016).
- [16] I. A. Sergienko and E. Dagotto, Role of the dzyaloshinskii-moriya interaction in multiferroic perovskites, *Physical Review B* **73**, 094434 (2006).
- [17] T. Aoyama, K. Yamauchi, A. Iyama, S. Picozzi, K. Shimizu, and T. Kimura, Giant spin-driven ferroelectric polarization in tbmno3 under high pressure, *Nature Communications* **5**, 4927 (2014).
- [18] I. A. Sergienko, C. Şen, and E. Dagotto, Ferroelectricity in the magnetic e-phase of orthorhombic perovskites ivan, *Physical Review Letters* **97**, 227204 (2006).
- [19] S. Picozzi, K. Yamauchi, B. Sanyal, I. A. Sergienko, and E. Dagotto, Dual nature of improper ferroelectricity in a magnetoelectric multiferroic, *Physical Review Letters* **99**, 227201 (2007).
- [20] B. Lorenz, Y. Q. Wang, and C. W. Chu, Ferroelectricity in perovskite homn o3 and ymno3, *Physical Review B* **76**, 10.1103/PhysRevB.76.104405 (2007).
- [21] S. Hayami, Y. Yanagi, and H. Kusunose, Momentum-dependent spin splitting by collinear antiferromagnetic ordering, *Journal of the Physical Society of Japan* **88**, 123702 (2019).
- [22] L. Šmejkal, R. González-Hernández, T. Jungwirth, and J. Sinova, Crystal time-reversal symmetry breaking and spontaneous hall effect in collinear antiferromagnets, *Science Advances* **6**, eaaz8809 (2020).
- [23] L.-D. Yuan, Z. Wang, J.-W. Luo, E. I. Rashba, and A. Zunger, Giant momentum-dependent spin splitting in centrosymmetric low-z antiferromagnets, *Physical Review B* **102**, 014422 (2020).
- [24] L. Šmejkal, J. Sinova, and T. Jungwirth, Beyond conventional ferromagnetism and antiferromagnetism: A phase with nonrelativistic spin and crystal rotation symmetry, *Physical Review X* **12**, 031042 (2022).

- [25] H.-Y. Ma, M. Hu, N. Li, J. Liu, W. Yao, J.-F. Jia, and J. Liu, Multifunctional antiferromagnetic materials with giant piezomagnetism and noncollinear spin current, *Nature Communications* **12**, 2846 (2021).
- [26] I. I. Mazin, K. Koepernik, M. D. Johannes, R. González-Hernández, and L. Šmejkal, Prediction of unconventional magnetism in doped fcsb2, *Proceedings of the National Academy of Sciences* **118**, 1 (2021).
- [27] R. González-Hernández, L. Šmejkal, K. Výborný, Y. Yahagi, J. Sinova, T. Jungwirth, and J. Železný, Efficient electrical spin splitter based on nonrelativistic collinear antiferromagnetism, *Physical Review Letters* **126**, 127701 (2021).
- [28] J. S. Lim, D. Saldana-Greco, and A. M. Rappe, Improper magnetic ferroelectricity of nearly pure electronic nature in helicoidal spiral camn7o12, *Physical Review B* **97**, 045115 (2018).
- [29] See Supplemental Material at xx, which includes Refs.[31-34]. We provide first-principles computational details, covering a range of altermagnetic materials with spin-driven ferroelectricity, including both 3D and 2D systems, as well as the phase transition pathways and magnetoelectric coupling calculations.,.
- [30] T. Uyama, K. Mukai, and I. Yamada, High-pressure synthesis and electrochemical properties of tetragonal limno2, *RSC Advances* **8**, 26325 (2018).
- [31] G. Kresse and J. Furthmüller, Efficient iterative schemes for ab initio total-energy calculations using a plane-wave basis set, *Physical Review B* **54**, 11169 (1996).
- [32] S. L. Dudarev, G. A. Botton, S. Y. Savrasov, C. J. Humphreys, and A. P. Sutton, Electron-energy-loss spectra and the structural stability of nickel oxide: An LSDA+U study, *Physical Review B* **57**, 1505 (1998).
- [33] J. P. Perdew, K. Burke, and M. Ernzerhof, Generalized gradient approximation made simple, *Phys. Rev. Lett.* **77**, 3865 (1996).
- [34] G. Kresse and D. Joubert, From ultrasoft pseudopotentials to the projector augmented-wave method, *Physical Review B* **59**, 1758 (1999).
- [35] A. Edström and C. Ederer, Prediction of a giant magnetoelectric cross-caloric effect around a tetracritical point in multiferroic srmno3, *Physical Review Letters* **124**, 167201 (2020).
- [36] R. Gupta and R. K. Kotnala, A review on current status and mechanisms of room-temperature magnetoelectric coupling in multiferroics for device applications, *Journal of Materials Science* **57**, 12710 (2022).
- [37] J. Shah and R. K. Kotnala, Room temperature magnetoelectric coupling enhancement in mg-substituted polycrystalline gdfeo3, *Scripta Materialia* **67**, 316 (2012).
- [38] W. J. Casteel, A. P. Wilkinson, H. Borrmann, R. E. Serfass, and N. Bartlett, Preparation and structure of ruthenium tetrafluoride and a structural comparison with ruthenium trifluoride and ruthenium pentafluoride, *Inorganic Chemistry* **31**, 3124 (1992).
- [39] S. Becker and B. G. Müller, Vanadiumtetrafluorid, *Angewandte Chemie* **102**, 426 (1990).
- [40] J. W. Stout and H. E. Adams, Magnetism and the third law of thermodynamics. the heat capacity of manganous fluoride from 13 to 320°k., *Journal of the American Chemical Society* **64**, 1535 (1942).
- [41] W. H. Baur and A. A. Khan, Rutile-type compounds. iv. sio2, geo2 and a comparison with other rutile-type structures, *Acta Crystallographica Section B Structural Crystallography and Crystal Chemistry* **27**, 2133 (1971).
- [42] J. H. Park, H. M. Jang, H. S. Kim, C. G. Park, and S. G. Lee, Strain-mediated magnetoelectric coupling in batio3-co nanocomposite thin films, *Applied Physics Letters* **92**, 062908 (2008).
- [43] H. Zhao, H. Kimura, Z. Cheng, M. Osada, J. Wang, X. Wang, S. Dou, Y. Liu, J. Yu, T. Matsumoto, T. Tohei, N. Shibata, and Y. Ikuhara, Large magnetoelectric coupling in magnetically short-range ordered bi5ti3feo15 film, *Scientific Reports* **4**, 5255 (2014).
- [44] H. J. Zhao, L. Bellaiche, X. M. Chen, and J. Íñiguez, Improper electric polarization in simple perovskite oxides with two magnetic sublattices, *Nature Communications* **8**, 14025 (2017).
- [45] C. Ederer and N. A. Spaldin, Weak ferromagnetism and magnetoelectric coupling in bismuth ferrite, *Physical Review B* **71**, 060401 (2005).